Article

Methanol Oxidation over Co- and/or Ag-Based Catalysts: Effect of Impurities (H_2O and CO)

Eleni Pachatouridou , Angelos Lappas , Eleni Iliopoulou *

Posted Date: 16 October 2025

doi: 10.20944/preprints202510.1314.v1

Keywords: Silver; Cobalt; Palladium; Platinum; Spray impregnation; Stability; H_2O; CO; methanol oxidation; reaction pathway

 doi:10.20944/preprints202510.1314.v1

Article

Methanol Oxidation Over Co- and/or Ag-Based Catalysts: Effect of Impurities (H_2O and CO)

Eleni Pachatouridou, Angelos Lappas and Eleni Iliopoulou *

Chemical Process and Energy Resources Institute (CPERI), Centre for Research and Technology Hellas (CERTH), Thermi, GR-57001 Thessaloniki, Greece

* Correspondence: eh@certh.gr; Tel.: +30 2310498312

Abstract

The methanol oxidation reaction was investigated on Co- and/or Ag-based γ-Al_2O_3 catalysts, which were prepared by different methods and further doped with noble metals (Pd, Pt). During the present study, three different reaction pathways were revealed. Complete oxidation of methanol to CO_2 and H_2O was achieved over Pd-doped catalysts (Pd-Co/Al-SI and Pd-Ag/Al-SI), while partial oxidation to intermediates, such as formaldehyde, was observed for Ag/Al catalysts. The dehydration reaction of methanol to dimethyl ether took place over Co/Al, Ag-Co/Al and Pt-Co/Al catalysts. The 0.5wt.% Pd-5wt.% Co/γ-Al_2O_3 catalyst, prepared via the spray impregnation (SI) method, exhibited the highest methanol oxidation efficiency (T_{50}: 43°C) and was further evaluated in the presence of H_2O and CO in the feed, for several hours on stream. Initially, the activity of the catalyst was decreased, while over time complete oxidation of methanol was achieved. Characterization of the used catalyst revealed that in addition to the Co_3O_4 phase initially formed in the fresh catalyst, a CoO phase was also formed, concluding that the active phase of the 0.5Pd-5Co/Al-SI catalyst for the methanol oxidation reaction is a mixture of Co_3O_4 and CoO phases.

Keywords: methanol oxidation; silver; cobalt; palladium; platinum; spray impregnation; stability; H_2O; CO

1. Introduction

Methanol (MeOH or CH_3OH) has received considerable attention in different fields worldwide, due to its low production cost, safety and properties [1,2]. Industrially, methanol is produced by synthesis gas and from other carbon-based feedstocks and processes, such as coal gasification, biomass gasification and direct synthesis from CO_2 [3,4].

In petrochemical industry, methanol is used as a feedstock for the production of chemicals, such as formaldehyde [5], acetic acid [6], plastics and resins, like poly(ethene) and poly(propene) [7,8]. Furthermore, CH_3OH is considered an excellent candidate for hydrogen generation and has received global attention as an alternative environmentally friendly fuel in industries, transportation, shipping and fuel cell applications, due to its lower flammability and its toxicity, which is comparable to or better than gasoline [3,9–13]. Some of the properties and characteristics that make methanol an attractive molecule is that it is liquid at standard temperature and pressure (STP), which means it can be easily stored and transported, with low carbon-to-hydrogen molar ratio, low combustion temperature, high flame speed and elevated knock resistance [14].

From an environmental perspective, methanol has many benefits, such as lower greenhouse gas emissions compared to gasoline and diesel and reduced air pollution. CH_3OH combustion produces less particulate matter, soot, SOx and NOx [15]. However, it is worth mentioning that partial methanol combustion can lead to the emission of other harmful products, such as formaldehyde (HCHO), carbon monoxide (CO) and unburned methanol vapors [16]. The complete methanol oxidation reaction (MOR) produces CO_2 and H_2O, so it is a great challenge to develop catalysts resistant to water vapor, as it can affect the active sites of the catalysts [17]. Hence, the composition

 doi:10.20944/preprints202510.1314.v1

of the exhaust gases can be complex and may contain impurities, like unburnt methanol, CO, H_2O and CO_2 [18–21]. Therefore, it is very important to develop a catalyst with the appropriate properties that will allow the complete oxidation of methanol even in the presence of these impurities.

Transition metals (Co, Fe, Mn, Au, Ag, etc.) based on a support (Al_2O_3, CeO_2, LiO_2, etc.) seem to be promising catalysts for the oxidation of volatile organic compounds (VOCs) [6,21–24]. The redox properties, the metal-support interaction and the promotion with noble metals (Pd, Pt) play a crucial role for the catalyst performance [20,21,25,26]. Cobalt (Co) due to its electronic and magnetic properties is used in a variety of reactions in energy and environmental sectors [27]. In methanol oxidation reaction, the mechanism of the reaction depends on the oxidation state of cobalt (Co_3O_4, CoO) and the CH_3OH to O_2 ratio. Zafeiratos et al. [24] revealed that over Co_3O_4 species, methanol is oxidized to CO_2 and H_2O, over CoO partial oxidation to HCHO takes place, while metallic cobalt is oxidized to CoO in methanol rich environments. Silver (Ag) on the other side is widely used in various selective catalytic oxidation reactions carried out in the chemical industry, like catalytic oxidation of methanol to HCHO [28,29]. Jablonska et al. [30] tested different metals, like Cu, Mn, Ag and bimetallic systems on γ-Al_2O_3 support for methanol incineration and concluded that the samples loaded with 1wt.% Ag presented the highest activity due to the dispersed Ag^+ species on alumina.

Among the studied catalytic supports, CeO_2 has received considerable attention due to its unique characteristics, such as high oxygen storage capacity, oxygen mobility and redox properties [20,31,32]. On the other side, γ-Al_2O_3 is cheaper, with high surface area, while the synergy potential of metal active sites - support, in combination with the dispersion of metal species on alumina tend to enhance the final catalytic efficiency [33]. Noble metals, especially Pt and Pd have also shown high activity for oxidation reactions at low temperature, due to the synergy of noble metal with the support, which increased the reducibility of the catalyst [21,25,34,35]. For the combustion of VOCs, Pd-based catalysts are preferred, since they present also resistant to moisture and sintering [35–38].

In a recent study [39], we have investigated the catalytic oxidation of CO and CH_3OH over Pd/Co-alumina catalysts. In detail, the catalysts were prepared using different cobalt loadings (1wt.% and 5wt.%) and synthesis methods (the conventional wet impregnation WI and the advanced spray impregnation SI technique). The superiority of spray impregnation method was clear for both oxidation reactions, due to the formation of core-shell catalytic nanostructures and the deposition of Co_3O_4 on the outer surface of the γ-Al_2O_3 support, securing the chemical/thermal stability of active sites on the catalyst carrier. Palladium (0.5wt.%) incorporation on 5 wt.% Co/γ-Al_2O_3 prepared by spray impregnation boosted the MOR, achieving a light-off temperature of 48 °C (T_{50}) and a complete conversion temperature of 64 °C (T_{90}).

The present work aims to investigate further the performance of doped Co-based catalysts on MOR, via incorporation of noble metals (0.1wt.%, 0.5wt.% loading), like Pt or Pd and transition metals, such as Ag (2wt.%). Additionally, Ag-based alumina catalysts were prepared applying either wet and/or spray impregnation methods, to compare them with bare Co-based catalysts. The optimum catalyst was further tested concerning its stability in the presence of impurities, such as H_2O and CO, and time-on-stream. The catalysts were fully characterized fresh (as prepared) and used (after reaction) in order to evaluate the effect of the synthesis method, reaction conditions and impurities on the catalytic properties.

2. Results

2.1. Textural and Structural Properties of Fresh Catalysts

Table 1 presents the textural properties of all as received/prepared catalytic materials (γ-Al_2O_3 support, Ag- and/or Co-based alumina catalysts, doped with Pt or Pd), such as metal content, surface area, pore volume, pore size and the crystallite size of the formed Co_3O_4, calculated via Scherrer equation from the peak at 2θ: 35-38° from the XRD patterns (Figure 1a). The metal content measured by ICP, revealed a Co content of approximately ~ 5.5 wt.%, while the high and low Pd-doped catalysts contained ~ 0.58 wt.% and 0.12 wt.% respectively and the corresponding Pt loading was ~0.6 wt.%

 doi:10.20944/preprints202510.1314.v1

and 0.17 wt.%. The silver content ranged between ~ 5.5 - 5.9 wt.%, with ~ 0.47 wt.% Pd. It is worth mentioning the difference between the Pd loadings in the 0.5Pd-5Co/Al-SI and 0.5Pd-5Ag/Al-SI catalysts (0.58 wt.% and 0.47 wt.%, respectively). Regarding surface area, as expected, the addition of metals over alumina reduced the surface area of the carrier and increased the pore size.

Table 1. Textural properties of the fresh catalytic materials.

Catalyst	Metal content (wt.%)				Surface area (m^2/g)	Pore volume (cm^3/g)	Pore size (nm)	Co_3O_4 crystallite size (nm) [ii]
	Co	Ag	Pd	Pt				
γ-Al_2O_3	**-**	**-**	-	-	238.2	0.61	10.3	-
5Co/Al-SI [i]	5.50	-	-	-	203.4	0.56	11.1	36.7
0.1Pd-5Co/Al-SI	5.40	-	0.12	-	208.2	0.58	10.8	31.5
0.5Pd-5Co/Al-SI [i]	5.46	-	0.58	-	210.1	0.57	10.8	30.0
0.1Pt-5Co/Al-SI	5.40	-	-	0.17	202.7	0.56	10.8	35.1
0.5Pt-5Co/Al-SI	5.40	-	-	0.60	203.1	0.56	10.7	31.8
2Ag-5Co/Al-SI	5.10	1.80	-	-	203.8	0.56	10.7	38.4
5Ag/Al-WI	-	5.90	-	-	202.7	0.58	10.0	-
5Ag/Al-SI	-	5.48	-	-	200.4	0.57	11.4	-
0.5Pd-5Ag/Al-SI	-	5.47	0.47	-	210.0	0.56	10.6	-

[i] Second batch of the fresh 5Co/Al-SI and 0.5Pd-5Co/Al-SI catalysts presented in [39]. [ii] Calculated applying Scherrer equation (1) at X-ray diffractograms (peak at 2θ: 35-38°).

In the case of Co-based catalysts, the crystallite size of Co_3O_4 was estimated from the XRD diffractograms (Figure 1a). In addition to the classic peaks of γ-alumina carrier (at 2θ: 37.2°, 45.6° and 67.2° based on JCPDS reference no. 00-010-0425 for γ-Al_2O_3), the Co-based catalysts exhibit intense peaks due to the formation of Co_3O_4 at 2θ: 19°, 31.3°, 36.8°, 44.8°, 55.6°, 59.3° and 65.2° [40]. For the undoped Co/Al catalyst prepared via the SI method, the crystallite size was calculated to be 36.7 nm, while the addition of Pt decreased the crystallite size to 35.1 nm and 31.8 nm, for the catalysts with 0.1 wt.% and 0.5 wt.% Pt, respectively. Further reduction in the size of Co_3O_4 was revealed for the Pd-doped cobalt catalysts, with crystallite sizes 31.5 nm for the 0.1Pd-5Co/Al-SI and 30 nm for the 0.5Pd-5Co/Al-SI. One the other hand, the XRD patterns of the Ag-based catalyst (Figure 1b) did not reveal any peak due to any silver phase (Ag_2O, Ag^0), possibly due to the efficient dispersion of Ag over the alumina carrier or the formation of small Ag-based particles. Even the different synthesis method did not affect the metal deposition on γ-Al_2O_3. Furthermore, the XRD pattern of the Ag-doped Co catalyst (2Ag-5Co/Al-SI), did not show any Ag peak, while the Co_3O_4 crystallite size was the highest (38 nm) measured. For the noble metal - doped catalysts (Pt or Pd), only one low intensity peak was observed for the catalysts with a Pd content of 0.5 wt.%, at 2θ: 33.8° attributed to the fromation of PdO phase [41].

 doi:10.20944/preprints202510.1314.v1

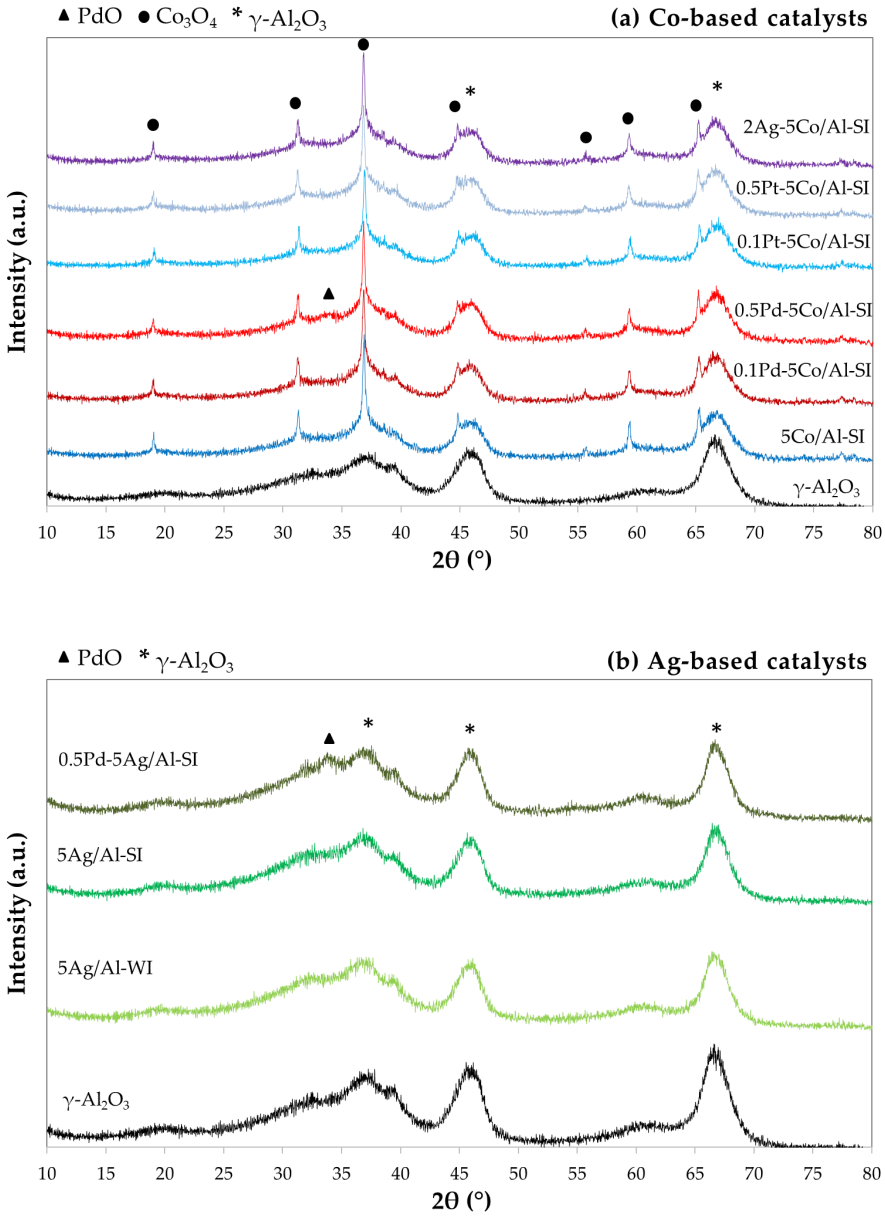

Figure 1. XRD patterns of the fresh (a) Co-based and (b) Ag-based catalytic materials.

So far, the synthesis method (WI vs. SI) has not shown any effect on the properties of the derived silver-based catalysts. As well known, SEM images provide a better understanding of the metals deposition on alumina carrier. Indeed, in our previous study [39], the SEM image of 5Co/Al-SI revealed the formation of a core–shell nanostructure, where Co_3O_4 was deposited on the outer surface of alumina particle. Besides Pd addition at different loadings, the catalyst, in the current study, was also doped with Ag (2 wt.%) and Pt (0.1 wt.% and 0.5 wt.%Pt).

In the case of Ag-based catalyst prepared by WI and SI methods, no significant differences were observed in SEM images concerning Ag deposition on the alumina carrier (Figure 2a and 2b, respectively). The silver deposition occurred homogeneously on the alumina particle, without creating the core-shell structure formed via spray impregnation method, as in the case of 5Co/Al-SI catalyst (Figure 2c). This fact is probably related to the mobility of Ag over the alumina particle during synthesis and more specifically during the thermal treatment (calcination at 500°C under air flow) of the material. Keijzer et al. [42] showed an increase in Ag particle size during oxidative thermal treatment up to 400°C. Even during a reaction/process, such as ethylene epoxidation [42] or methanol oxidation to formaldehyde [43], changes in the morphology of the silver active sites are possible due to the mobility of Ag species. SEM images of the 2Ag-5Co/Al-SI catalyst revealed the formation of a

 doi:10.20944/preprints202510.1314.v1

core-shell structure of Co deposition on alumina carrier, while Ag species (via dry impregnation method) were widely and uniformly dispersed on alumina carrier.

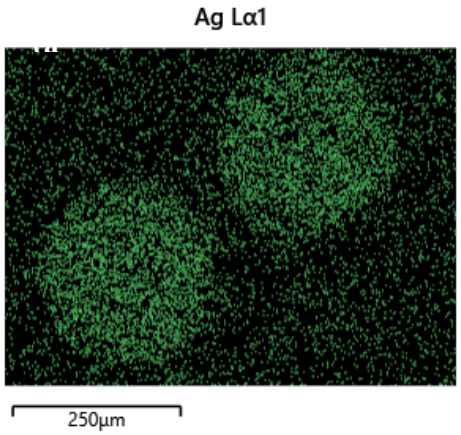

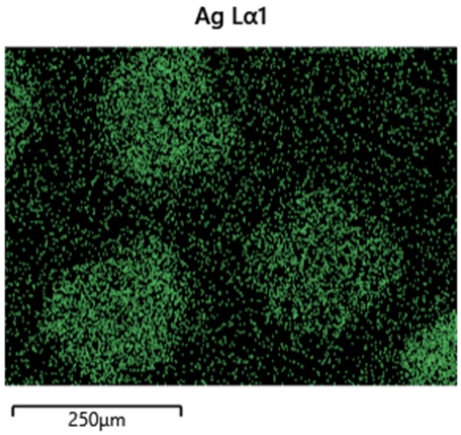

 doi:10.20944/preprints202510.1314.v1

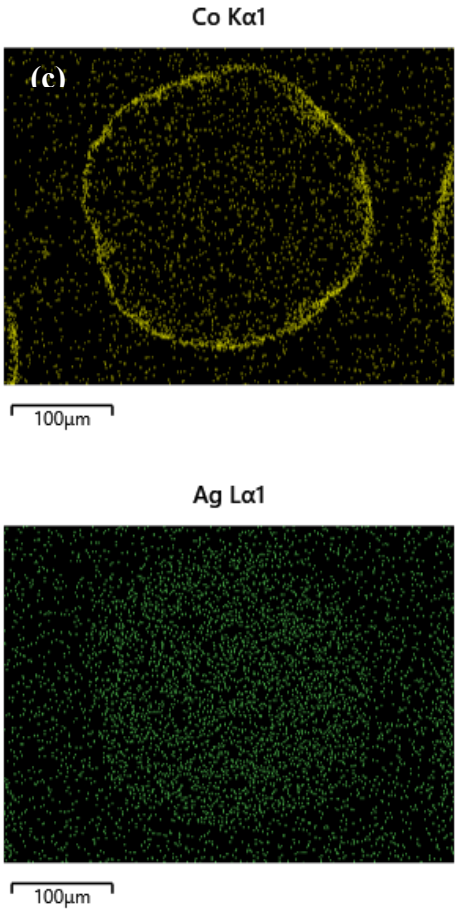

Figure 2. SEM images of metals deposition (Co: yellow dots, Ag: green dots) on alumina particles for (a) 5Ag/Al-WI, (b) 5Ag/Al-SI and for 2Ag-5Co/Al-SI the deposition of (c) Co and (d) Ag.

2.2. Reducibility of Fresh Catalysts

Structural characterization revealed the formation of Co_3O_4 species over cobalt-based catalysts, while in the case of silver-based catalysts the oxidation state of Ag is not clear. Thus, the reducibility of the Ag-based catalysts was investigated via TPR-H_2 and the reduction profiles are presented in Figure 3. The corresponding reduction profiles for the cobalt catalysts were presented in Iliopoulou et al. [39], where two main reduction peaks were observed, related to the reduction of Co_3O_4 to CoO (low temperature peak) and the reduction of CoO to Co^0 (high temperature peak) respectively. Moreover, the addition of Pd shifted the reduction profiles to lower temperatures, indicating a significant increase in the reducibility of the catalysts.

As shown in Figure 3, the 5Ag/Al-WI catalysts exhibit two low intensity peaks at 110°C and 170°C, and two broad peaks at 300°C and 600°C. The low temperature peaks are related to the reduction of large Ag_2O clusters, while at higher temperatures (> 300°C) the reduction of small Ag_2O clusters takes place. The silver catalyst prepared with SI method (5Ag/Al-SI) and the Pd-doped catalyst (0.5Pd-5Ag/Al-SI) present similar reduction profiles, with some differences in the intensity of the peaks. A main, low temperature, broad peak with A maximum at 100-130°C and two broad peaks centered at 250-300°C and at temperatures above 500°C are observed, attributed to large Ag_2O clusters and well-dispersed smaller Ag_2O [44,45].

 doi:10.20944/preprints202510.1314.v1

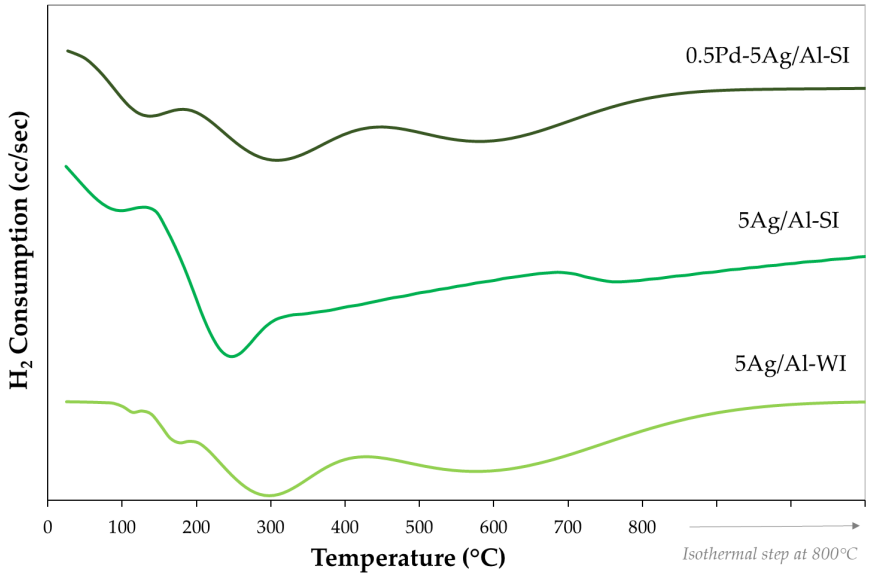

Figure 3. Reduction profiles of Ag-based catalysts (5Ag/Al-WI, 5Ag/Al-SI and 0.5Pd-5Ag/Al-SI).

2.3. Methanol Oxidation Reaction

2.3.1. Effect of Noble and Transition Metals on Co-Based Catalysts

Methanol oxidation performance of doped cobalt-based catalysts is shown in Figure 4. The superiority of the 0.5Pd-5Co/Al-SI catalyst is obvious, achieving 50% methanol conversion at 43°C (T_{50}), while the decrease of the Pd content in the Pd-Co catalyst to 0.1wt.% (0.1Pd-5Co/Al-SI) shifted the conversion plot to higher temperatures with T_{50}: 95°C, maintaining the superiority even compared to the Pt-doped Co/Al catalyst (Pt content of 0.5wt.%) presenting T_{50}: 119°C. Decreasing the Pt content to 0.1wt.% did not affect the catalyst performance, presenting almost similar plots (T_{50}: 126°C). On the other hand, the incorporation of 2 wt.% Ag did not improve the methanol oxidation activity of 5Co/Al-SI, but remained the same or slightly reduced it, shifting T_{50} from 191°C for 5Co/Al-SI to 198°C for 2Ag-5Co/Al-SI. In the literature, the combination of silver and cobalt on alumina carrier resulted in synergistic interaction of these metals, demonstrating high activity for CO oxidation reaction, which was affected by catalyst synthesis method [46]. In the methanol oxidation reaction, the combination of Ag and Co did not have the same effect. Probably the deposition of Co on the outer surface of the alumina particles (when applying spray impregnation) and then the incorporation of 2wt.% Ag using the dry impregnation method, dispersed silver all over the alumina particles as revealed SEM images (Figure 2c and d), without creating the expected synergy between Co-Ag.

 doi:10.20944/preprints202510.1314.v1

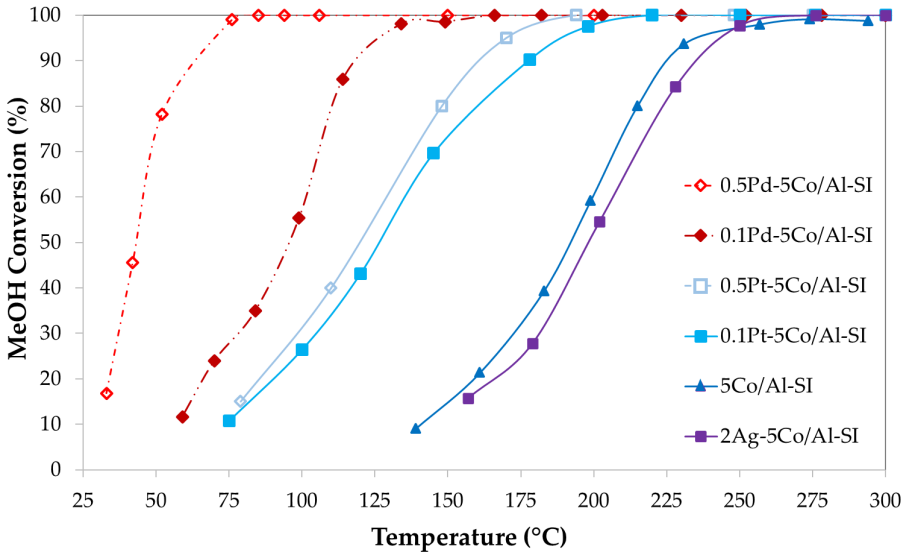

Figure 4. Methanol conversion plots for doped Co/γ-Al_2O_3-SI catalysts *(Experimental conditions: 0.1 vol.% CH_3OH-0.1 vol.% O_2)*.

Figure 5 present the MOR products for 0.5Pt-5Co/Al-SI, 2Ag-5Co/Al-SI and 0.1Pt-5Co/Al-SI (Fig. 5a, 5b and 5c, respectively). Different reaction pathways appear to be followed by each catalyst. The Pt-doped cobalt catalysts (same products despite different Pt loading) at high reaction temperatures of 225-300°C oxidized methanol to CO_2 and H_2O, while at lower temperatures (T < 225°C) dimethyl ether and formaldehyde were produced from MOR. The addition of Ag on Co/Al catalyst presented similar products with bare 5Co/Al-SI catalyst [39], but with lower concentration of DME and similar concentration of HCHO. This implies that the reaction follows the same mechanism with 5Co/Al-SI catalyst. The catalyst with low Pd content of 0.1wt.% (Fig. 5c) mainly produce CO_2 and H_2O during methanol oxidation reaction at the temperature range of 115-300°C, while at lower temperatures the formation of HCHO (maximum concentration of 55 ppm) was observed in higher concentrations than the corresponding catalyst with 0.5wt.% Pd, where traces of formaldehyde were detected [39]. The different products revealed different reaction mechanisms for each catalyst and for this reason bare 5wt.% Ag on γ-Al_2O_3 was prepared (applying both wet and spray impregnation methods), in order to study silver performance in MOR.

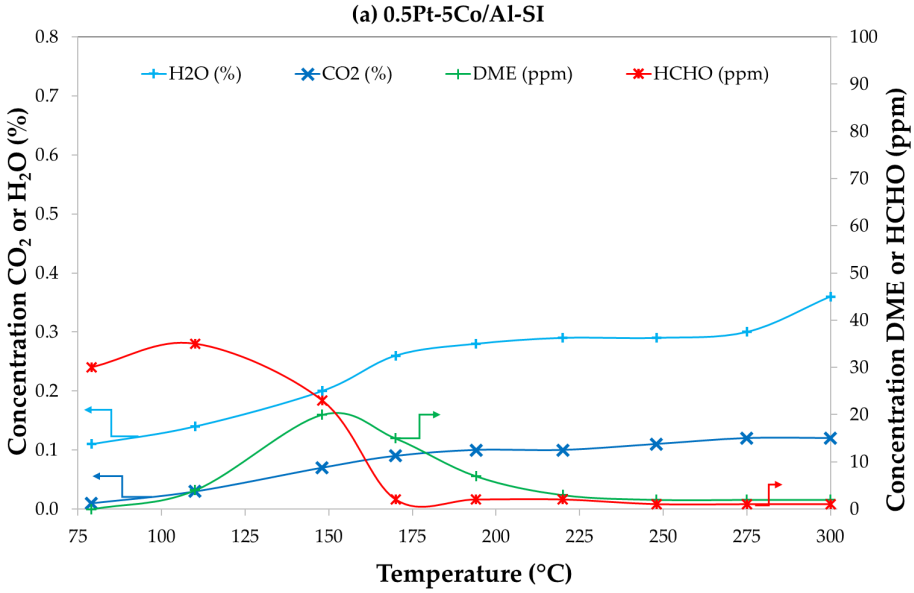

 doi:10.20944/preprints202510.1314.v1

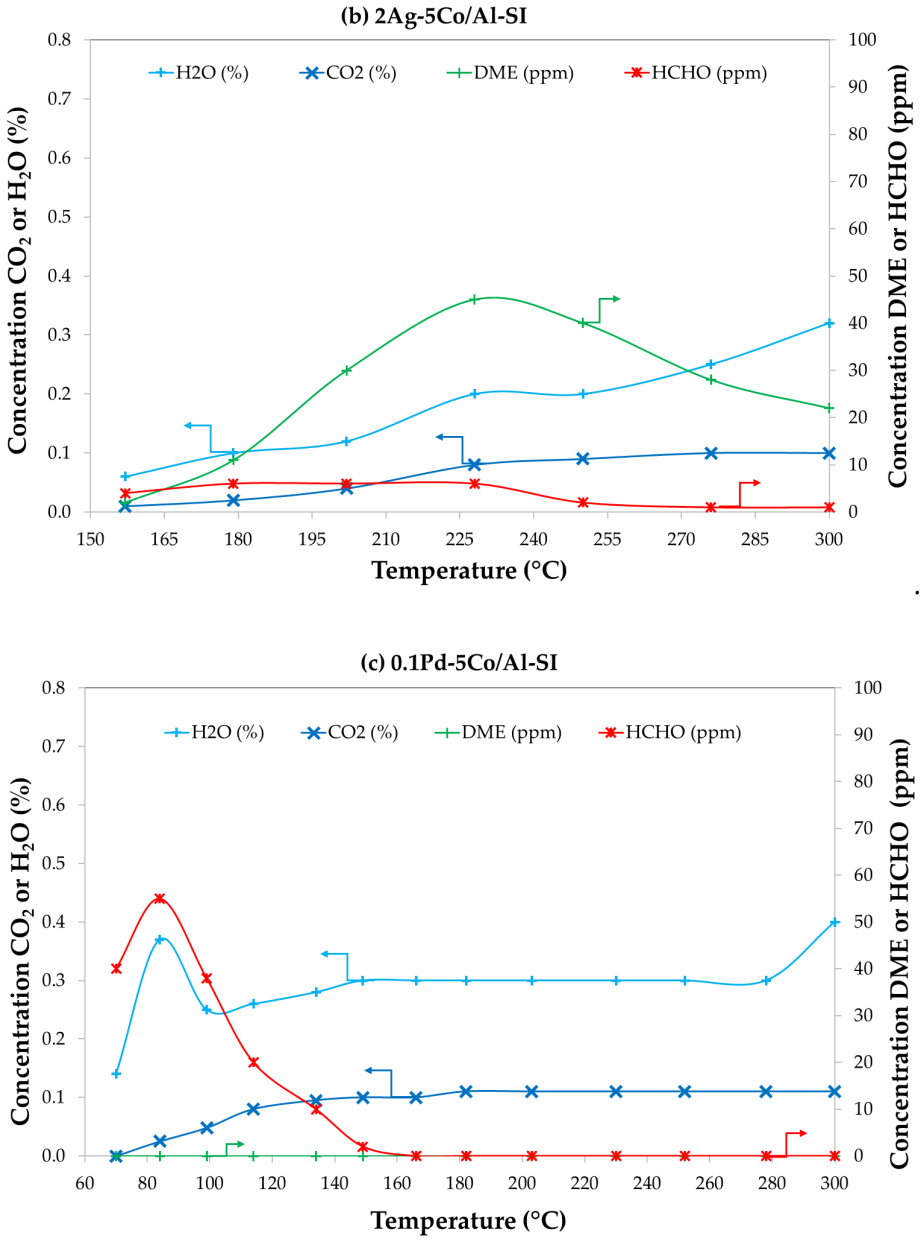

Figure 5. Products from methanol oxidation reaction for (a) 0.5wt.% Pt-, (b) 2wt.% Ag- and (c) 0.1wt.% Pt-doped 5Co/Al-SI catalysts *(Experimental conditions: 0.1 vol.% CH_3OH-0.1 vol.% O_2).*

2.3.2. Effect of Synthesis Method and Pd-Doping on Ag-Based Catalysts

Silver is widely used for methanol oxidation to formaldehyde, but also has studied for the oxidation of volatiles organic compounds to CO_2 and H_2O, like formic acid, acetic acid, ethanol, etc. [47]. Thus, instead of using silver as a dopant for Co/Al catalyst, Ag-based alumina catalysts were prepared applying both wet and spray impregnation methods. In Figure 6, it is obvious that there is no significant difference in the methanol oxidation performance of the differently prepared silver catalysts, as the 5Ag/Al-WI and -SI catalysts present similar conversion plots. These results agree with their structural characterization (XRD patterns in Figure 1b and SEM images in Figure 2a, b), where the synthesis method did not affect catalysts' properties, presenting similar structures. In the case of Co-based catalysts, important differences were observed between the catalysts and the difference in T_{50} was ~ 23°C between the two differently synthesized Co-based samples [39], while in silver-based catalysts is only 10°C. However, the silver-based catalysts present higher methanol oxidation performance than cobalt-based catalysts, with 50% MeOH conversion at 137°C for 5Ag/Al-SI and at 191°C for 5Co/Al-SI.

 doi:10.20944/preprints202510.1314.v1

Incorporation of 0.5wt.% Pd on 5Ag/Al-SI catalyst shifted the conversion plots to lower temperatures, enhancing the oxidation performance of bare silver catalysts, achieving T_{50} at 81°C. As compared with the doped-cobalt catalyst, the 0.5Pd-5Co/Al-SI (T_{50}: 43°C) presented the highest activity, followed by the 0.5Pd-5Ag/Al-SI (T_{50}: 81°C) and the 0.1Pd-5Co/Al-SI (T_{50}: 95°C). It seems that Pd (0.5 wt.%) improved the performance of the Co-based catalyst more than the Ag/alumina catalyst, despite the higher Pd content in the catalysts as shown in Table 1 (0.58 wt.% Pd for Co/Al and 0.47 wt.% Pd for Ag/Al), as the difference in ΔT_{50} between the 0.1Pd-5Co/Al-SI catalyst with 0.12 wt.% Pd content and the 0.5Pd-5Ag/Al-SI catalyst is 14°C, while between 0.5Pd-Co/Al-SI and 0.5Pd-5Ag/Al-SI is 38°C.

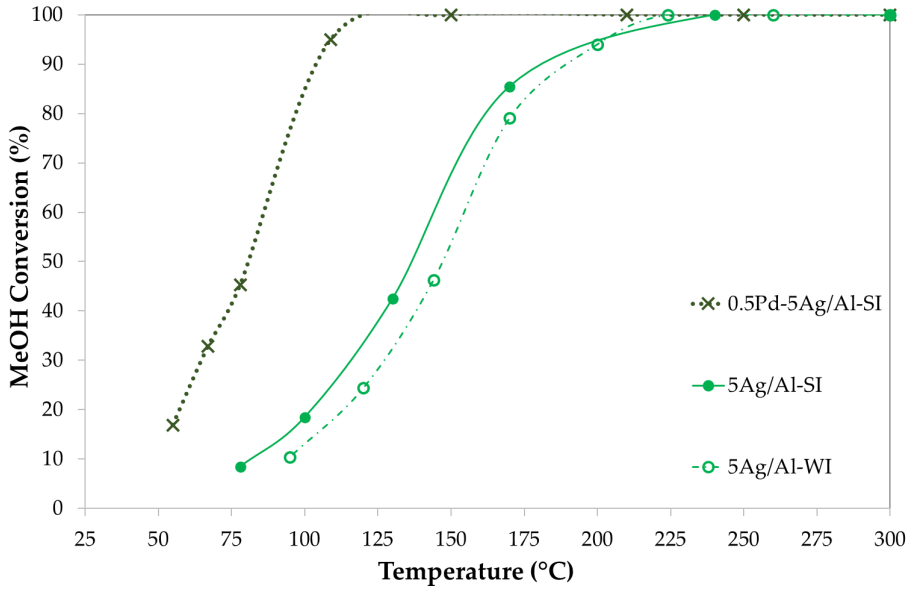

Figure 6. Methanol conversion plots for Ag/γ-Al_2O_3 prepared with WI and SI methods and Pd-doped Ag-based catalysts *(Experimental conditions: 0.1 vol.% CH_3OH-0.1 vol.% O_2).*

In the case of Ag-based catalysts different reaction mechanism seemed to take place based on the products of MOR (Figures 7). The production of CO_2 and H_2O was observed at the high temperature area (175-300°C), while at lower temperatures formaldehyde was detected, without the production of DME. The incorporation of Pd (Figure 7c) into the 5Ag/Al-SI catalyst changed the reaction mechanism and appears to be similar to the corresponding 0.5Pd-5Co/Al-SI catalyst, where when the methanol conversion started to decrease (T < 100°C) formaldehyde production was observed during MOR. So, it seems that the increase in catalytic activity of 5Ag/Al-SI catalyst was likely due to Pd, with Ag promoting formaldehyde formation.

 doi:10.20944/preprints202510.1314.v1

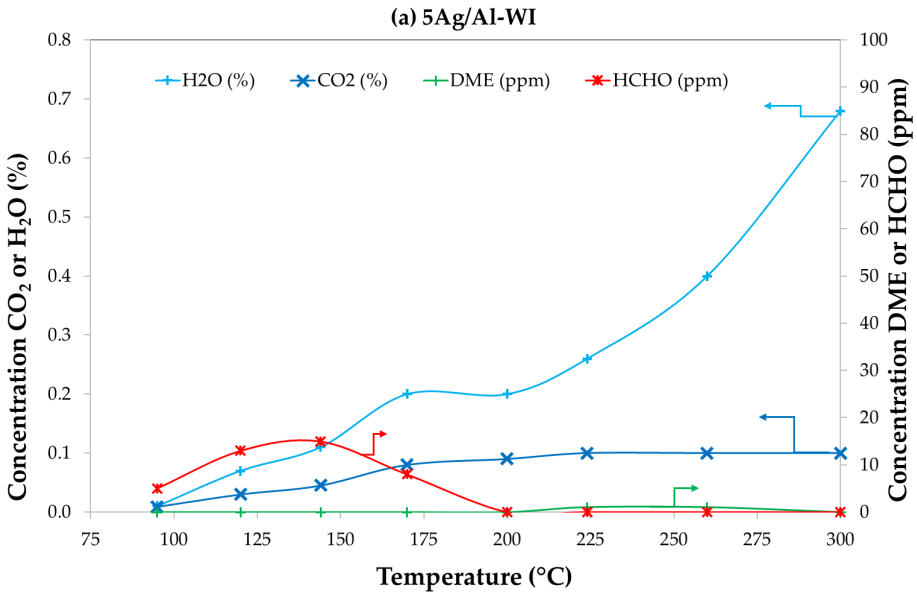

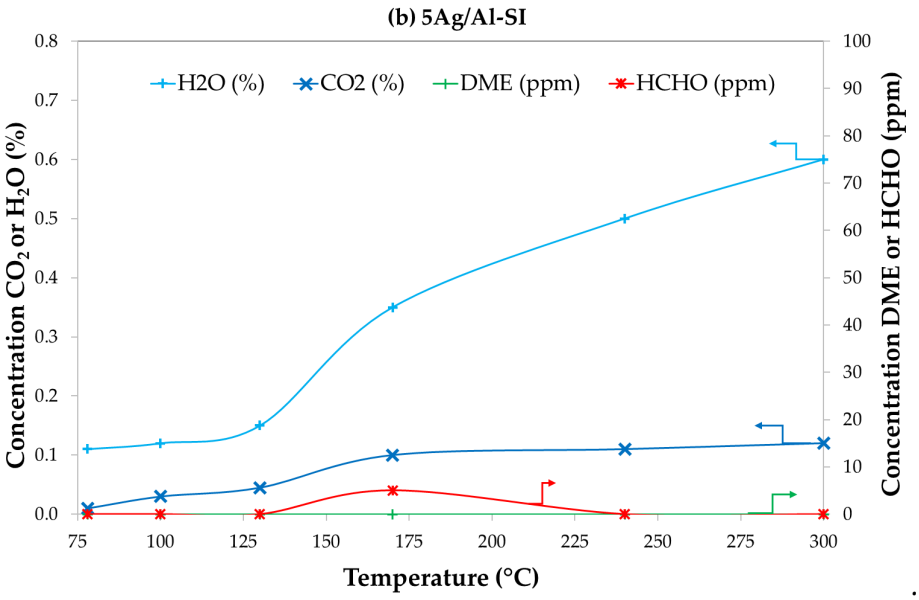

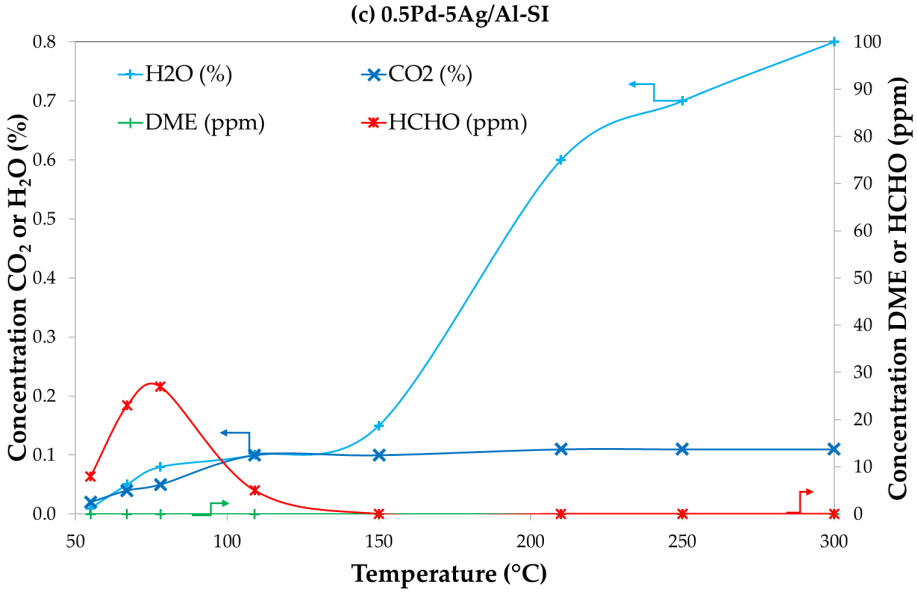

 doi:10.20944/preprints202510.1314.v1

Figure 7. Products from methanol oxidation for (a) 5Ag/Al-WI, (b) Ag/Al-SI and (c) 0.5Pd-5Ag/Al-SI *(Experimental conditions: 0.1 vol.% CH_3OH-0.1 vol.% O_2).*

2.4. Effect of Impurities (H_2O and CO) and Catalysts Stability with Time-on-Stream

2.4.1. Effect of CO and/or H_2O on Optimum 0.5Pd-5Co/Al-SI Catalyst Activity

The catalyst with the highest activity 0.5Pd-5Co/Al-SI was further tested for methanol oxidation reaction in the presence of CO and/or H_2O. Figure 8 presents the effect of the impurities on catalyst activity during light-off experiments. The addition of 2 vol.% H_2O in the feed *(Feed 2)* shifted conversion plots at higher temperatures and increased T_{50} from 43°C to 97°C, possibly due to the competitive adsorption of methanol and water on catalyst active sites, resulting in partial loss of activity [33]. The *Feed 3*, except CH_3OH, O_2 and H_2O contains 0.1vol.% CO and the catalytic performance of 0.5Pd-5Co/Al-SI is further diminished, presenting 50% methanol conversion at 203°C. In the presence of CO, it seems that CO and methanol are competing further for the catalyst's active sites, and probably the adsorption of methanol is poorer than CO, based on the CO conversion results (Figure 8). At T < 300°C, methanol conversion started to decrease, while CO conversion was increased achieving almost complete oxidation (~96%) at 220°C. This catalyst has been also tested for CO oxidation, showing high activity [39]. The coexistence of CO and MeOH (along with O_2 and H_2O) indicates a weaker sorption of methanol on the active sites of the 0.5Pd-5Co/Al-SI catalyst, as compared to the CO adsorption, which seems to be stronger, hindering the methanol adsorption.

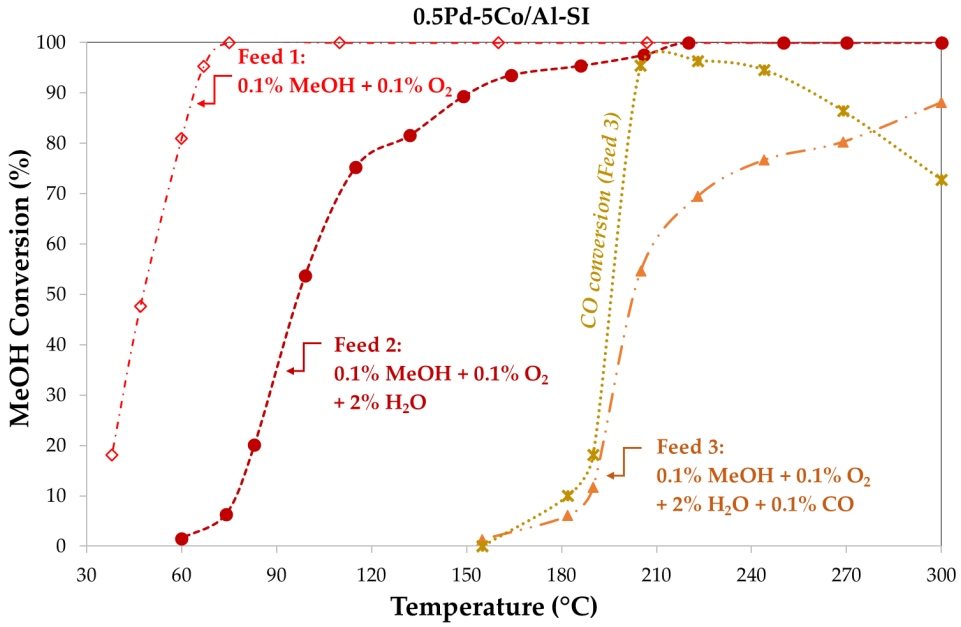

Figure 8. Methanol conversion plots for 0.5wt.% Pd-5wt.% Co/γ-Al_2O_3-SI in the presence of CO and/or H_2O *(Experimental Conditions-Feed 1: 0.1 vol.% CH_3OH-0.1 vol.% O_2, Feed 2: 0.1 vol.% CH_3OH-0.1 vol.% O_2-2 vol.% H_2O, Feed 3: 0.1 vol.% CH_3OH-0.1 vol.% O_2-2 vol.% H_2O-0.1 vol.% CO).*

2.4.2. Catalyst Stability with Time-on-Stream

Figure 9 shows the stability performance of the 0.5Pd-5Co/Al-SI catalyst for 12h TOS, under (*Feed 3*) 0.1 vol.% CH_3OH-0.1 vol.% O_2-2 vol.% H_2O-0.1 vol.% CO and at 230°C. The reaction temperature was chosen based on the catalyst performance in Figure 8 (under *Feed 3*), where the methanol conversion was approximately 75%. In the first 1h of the reaction, the methanol conversion was 80% and with TOS the conversion increased, reaching 94% after 9h MOR. In the last 3h of the reaction (t: 9-12h), the methanol conversion was increased further, achieving complete methanol conversion (100%). CO conversion ranged between 97-100% during the experiment and the main reaction

 doi:10.20944/preprints202510.1314.v1

products were CO_2 and H_2O, while traces (less than 3 ppm) of DME and formaldehyde were detected (Figure 10).

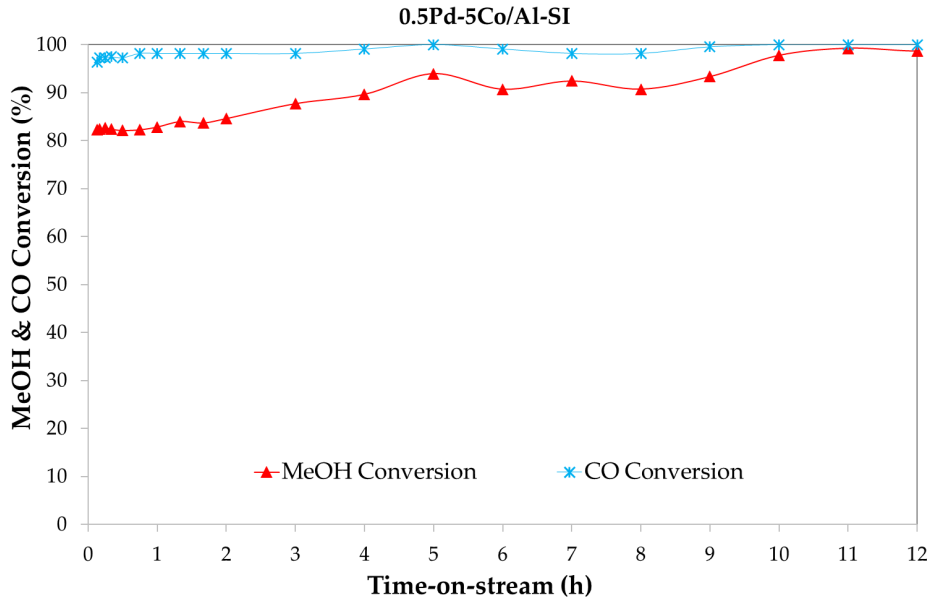

Figure 9. Catalyst 0.5wt.% Pd-5wt.% Co/γ-Al_2O_3-SI stability in the presence of impurities *(Experimental Conditions: 0.1 vol.% CH_3OH-0.1 vol.% O_2-2 vol.% H_2O-0.1 vol.% CO, Reaction temperature: 230°C, TOS: 12h).*

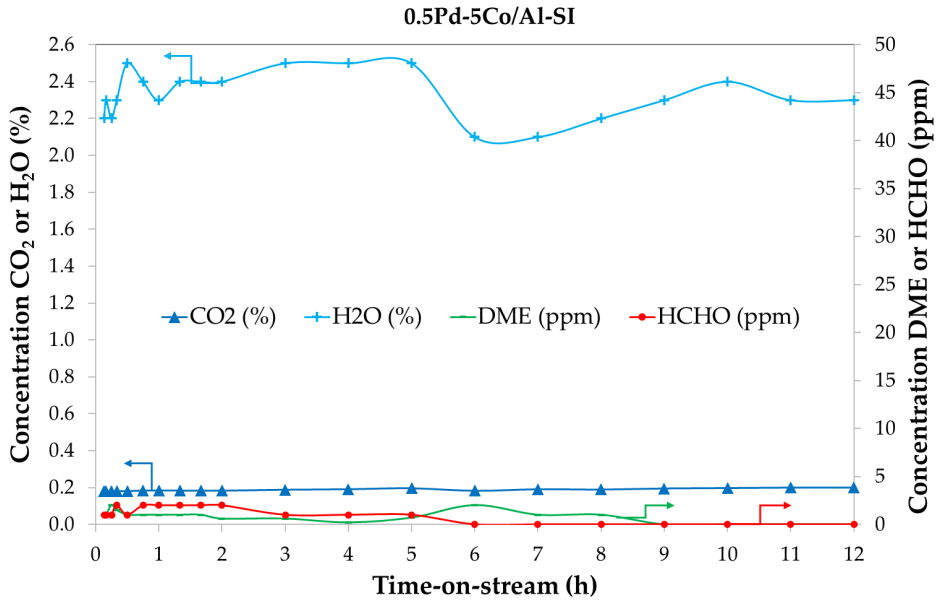

Figure 10. Products from stability experiment with 0.5wt.% Pd-5wt.% Co/γ-Al_2O_3-SI catalyst in the presence of impurities *(Experimental Conditions: 0.1 vol.% CH_3OH-0.1 vol.% O_2-2 vol.% H_2O-0.1 vol.% CO, Reaction temperature: 230°C, TOS: 12h).*

2.5. Physicochemical Characteristics of Used Catalysts

The improvement of the activity of the 0.5Pd-5Co/Al-SI catalyst during the stability experiment was investigated by characterizing the used catalyst via TPR-H_2 and XRD methods. The reduction profiles of fresh and used (after stability experiment) Pd-Co/Al-SI catalysts are shown in Figure 11. The fresh catalyst presents three peaks, with maximum at 160°C, 310°C and at 800°C. The first two peaks are assigned to the reduction of Co_3O_4 to CoO and then to metallic Co^0, and are shifted at lower

 doi:10.20944/preprints202510.1314.v1

temperatures compared to bare Co_3O_4 [32] or Co/γ-Al_2O_3 reduction profiles [39], due to the incorporation of Pd which enhance catalyst reducibility. The high temperature peak is assigned to the reduction of Co-Al species, like $CoAl_2O_4$, where there is a strong interaction of cobalt with alumina carrier [48]. The reduction profile of used catalyst presents the same peaks with the fresh one, but with differences in the intensities of H_2 consumption peaks. The intensity of the first peak (reduction of Co_3O_4 → CoO) is similar with the fresh one, while the intensity of the second peak (reduction of CoO → Co^0) is higher, which means that more CoO species existed in the used sample than the fresh one, which were formed in situ during the stability experiment.

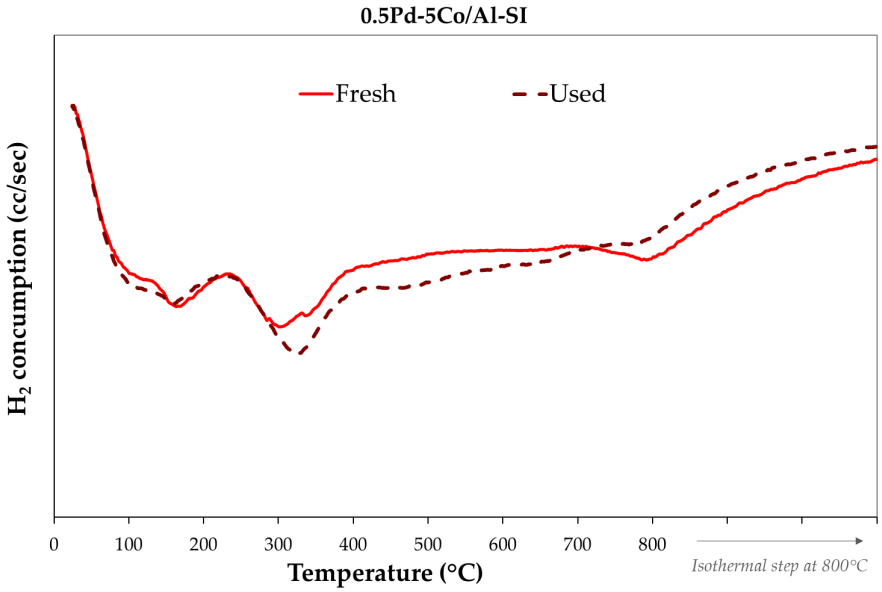

Figure 11. Reduction profiles of the fresh and used after stability experiment for 12h TOS of 0.5Pd-5Co/Al-SI catalyst.

The XRD patterns of fresh and used are compared in Figure 12 and confirm the conclusions from the reduction profiles. Significant differences are identified in the XRD diffractograms related to the oxidation state of both Co and Pd. The fresh catalyst, in addition to the peaks of γ-Al_2O_3, also showed peaks due to the formation of Co_3O_4 and PdO. The used catalyst present lower intensity Co_3O_4 peaks and no any PdO peak, while new peaks were formed due to CoO phase, at 2θ: 42.4°, 61.7°, 73.5° and 77.5° [49]. It seemed that under the reaction conditions (0.1 vol.% CH_3OH - 0.1 vol.% O_2 - 2 vol.% H_2O - 0.1 vol.% CO) and with TOS, significant structural changes occurred. Thus, it is likely that the active phase of the 0.5Pd-5Co/Al-SI catalyst for MOR is a mixture of Co_3O_4 and CoO phases. Zafeiratos et al. [24] studied two important parameters for methanol oxidation reaction, (i) the active phase of cobalt and (ii) the CH_3OH/O_2 mixing ratio. The methanol to O_2 ratio strongly affected the oxidation state of Co, which is a mixture of CoO and Co_3O_4 (CoOx) and the reaction mechanism.

 doi:10.20944/preprints202510.1314.v1

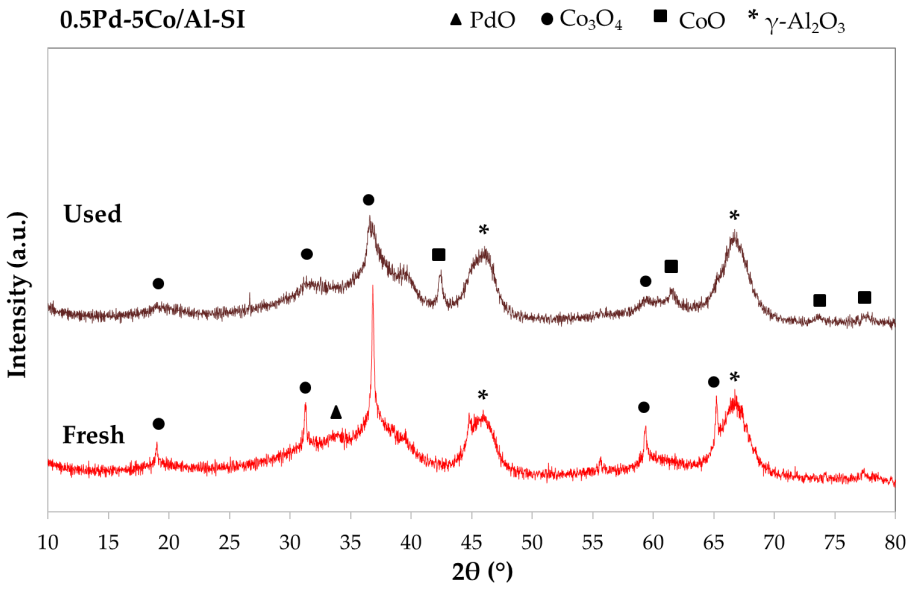

Figure 12. XRD patterns of the fresh and used after stability experiment for 12h TOS of 0.5Pd-5Co/Al-SI catalyst.

3. Discussion

The doping of Co/γ-Al_2O_3 catalyst, prepared with spray impregnation method, with noble metals (Pd or Pt) and/or a transition metal (Ag) revealed that each "combination" results in a different reaction pathway. Methanol desorption study offered an insight into the MOR mechanism, where the results are in full agreement with the results from catalysts' evaluation performance. Figure 13 (a-d) shows the MS signals of CO_2 (a-b), DME (c) and HCHO (d) desorbed from the saturated with methanol catalysts, under 0.1 vol.% O_2/He. The CO_2 desorption profiles of Co- (Figure 13a) and Ag-based (Figure 13b) catalysts present higher intensities as compared with DME and HCHO profiles. Bare 5Co/Al-SI catalyst exhibits one, low intensity, CO_2 peak at high temperatures (T > 220°C), similar with the 2Ag-5Co/Al-SI catalyst. The Pt- and Pd-doped cobalt catalysts present CO_2 desorption during the whole temperature range (RT – 300°C). The Pt-Co/Al catalyst present two temperature areas of CO_2 desorption, at 50 – 140°C and at 160 – 300°C, while Pd-Co/Al desorbed CO_2 during the whole range, with different peak intensities.

Bare 5Ag/Al catalyst prepared either with WI or SI method presents similar desorption profiles of CO_2 (T > 200°C), while the addition of Pd, desorbed CO_2 at lower temperatures starting from 100°C. The signal of DME (Figure 13c) was detected for 5Co/Al-SI, 2Ag-5Co/Al-SI and 0.5Pt-5Co/Al-SI catalysts, with similar intensities and temperature area (RT – 200°C), while formaldehyde (Figure 13d) signal was detected for all the catalysts, with higher intensities for Ag-based catalysts and 0.5Pt-5Co/Al-SI.

 doi:10.20944/preprints202510.1314.v1

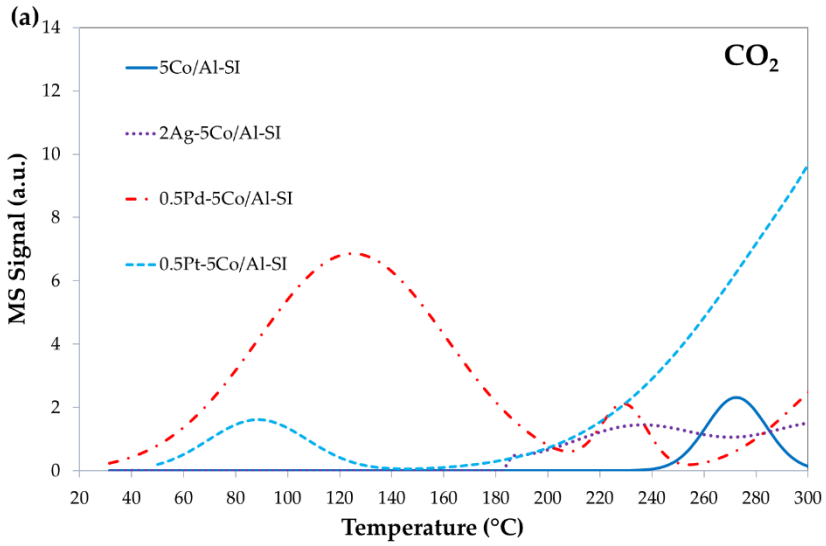

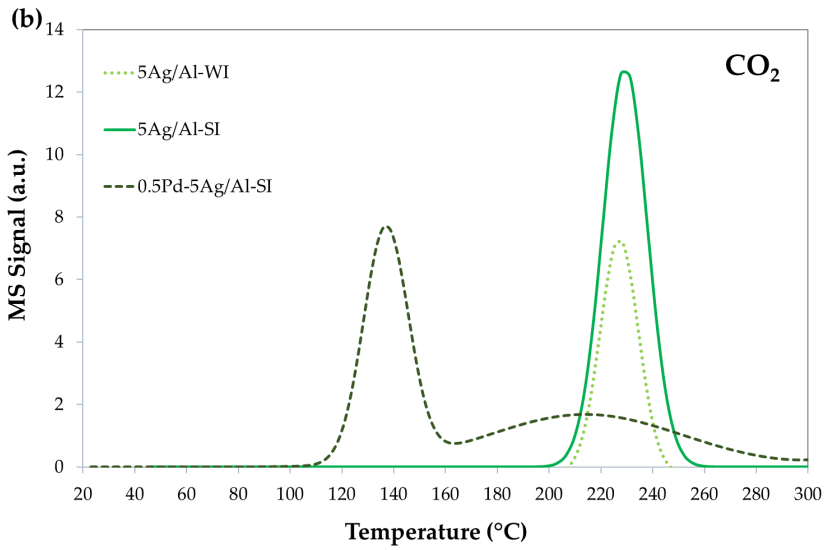

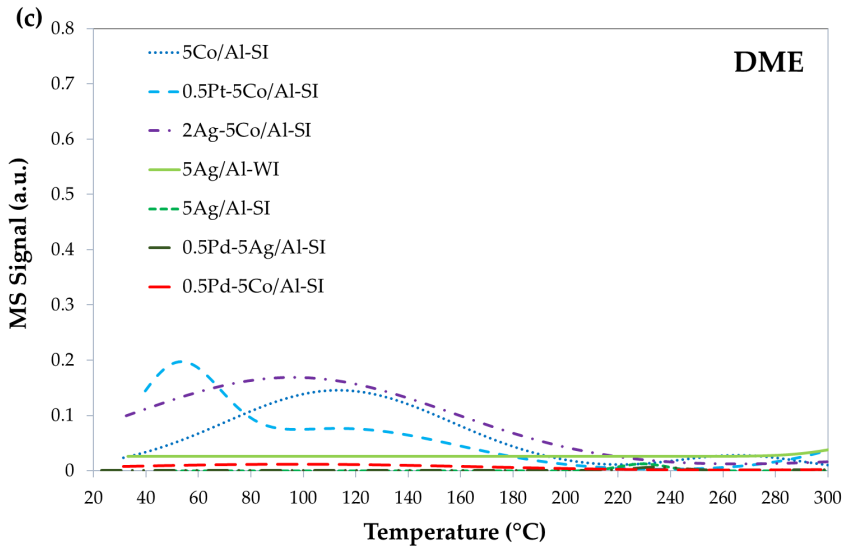

 doi:10.20944/preprints202510.1314.v1

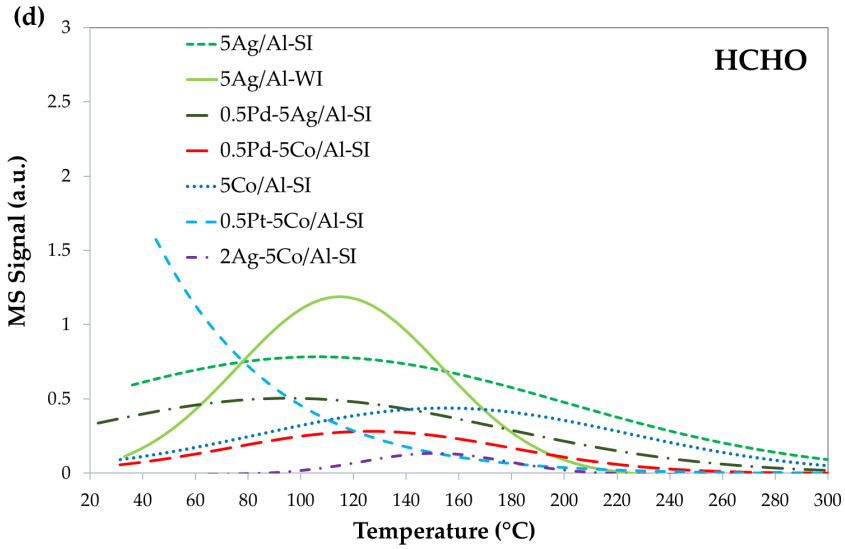

Figure 13. Methanol desorption study under 0.1 vol.% O_2/He for the investigated catalysts: (a) CO_2 for Co-based catalysts, (b) CO_2 for Ag-based catalysts, (c) DME and (d) HCHO for all catalysts.

Based on the literature, the initial step (I) during MOR is the formation of methoxy species (CH_3O-) through CH_3OH adsorption and dissociation on catalyst [24,33,50], while the next step and the different intermediates of MOR strongly depend on the metal and metal oxidation state [24]. Thus, three different reaction pathways were observed during the current study (Figure 14). The first one (A), is the complete oxidation of methanol to CO_2 and H_2O through dehydrogenation of methoxy species (complete oxidation), which takes place on Pd-doped catalysts (0.5Pd-5Co/Al-SI and 0.5Pd-5Ag/Al-SI), where the main reaction products were CO_2 and H_2O [43]. A second pathway (B), is the reaction of methoxy species with another methanol molecule (CH_3OH dehydration) producing DME, which was observed for 5Co/Al-SI, 2Ag-5Co/Al-SI and 0.5Pt-5Co/Al-SI catalysts [33,51]. The last one (C) pathway that may take place during MOR is the dehydrogenation of methoxy species to intermediates like formaldehyde, which can be followed by dehydrogenation/oxidation of intermediates to CO_2 and H_2O, was observed for Ag/Al and Pt-Co/Al catalysts [33,43].

It seems that Pd enhances the initial mechanism step, the formation of more methoxy species and in the case of the Ag catalyst it promotes pathway (C). On the other side, the characterization of the Pd-Co/Al catalyst revealed an interaction between the two metals, where Pd also improved the reducibility of the catalyst and reduced the size of the Co_3O_4 crystallites to 30 nm (Table 1), which leads to complete oxidation of methanol without the formation of intermediates. However, stability experiments revealed that the active cobalt phase is a mixture of Co_3O_4 and CoO, as revealed by the characterization of the used catalyst.

 doi:10.20944/preprints202510.1314.v1

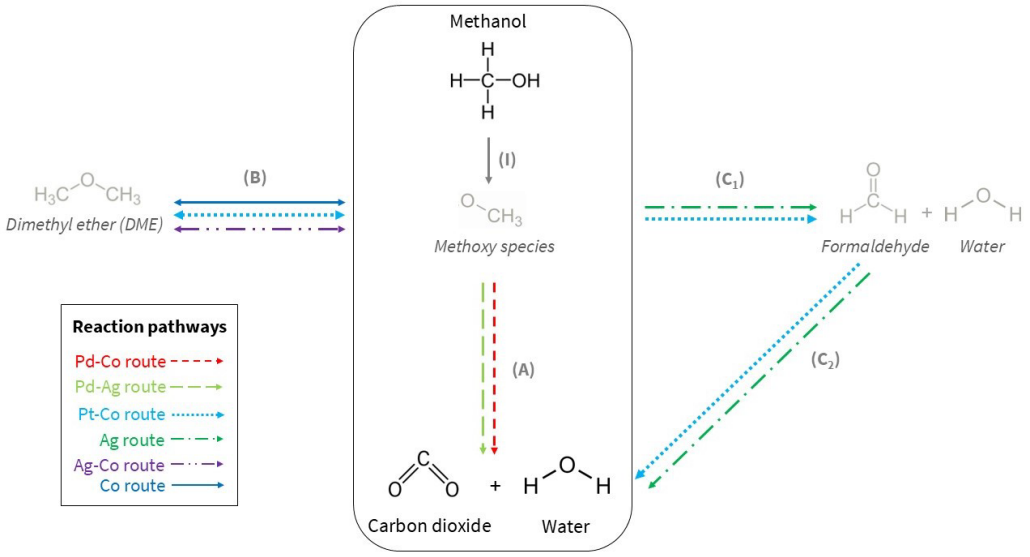

Figure 14. Main reaction pathways of methanol oxidation reaction for the investigated catalysts.

4. Materials and Methods

4.1. Catalyst Preparation

Different synthesis methods were used to prepare catalytic materials. Wet impregnation (WI) and spray impregnation (SI) were used to impregnate 5wt.% of the transition metal Co or Ag on alumina support (supplied by Saint Gobain NorPro), while incipient wetness impregnation method (dry impregnation, DI) was used for the incorporation of the transition metal Ag (2wt.%) and of low amounts (either 0.1wt.% or 0.5wt.%) of noble metals, such as Pd and Pt. The precursor salts were $Co(CH_3CO_2)_2{\cdot}4H_2O$ (purchased from Sigma-Aldrich with purity > 99%), $AgNO_3$ (supplied by Honeywell-Fluka and purity ≥ 99.8%), $Pd(NO_3)_2{\cdot}2H_2O$ (from Sigma-Aldrich) and $Pt(NH_3)_2(NO_2)_2$ (from Sigma-Aldrich). A detailed description of the synthesis methods of Co-alumina based catalysts doped or not with Pd, is presented in Iliopoulou et al. [39]. The same methods and conditions were used for the synthesis of bare Ag- alumina-based catalysts, doped or not with Pd. The catalysts are labeled as xN-5M/Al-z, where *x* is the loading of the noble/transition metal (0.1wt.%, 0.5wt.% or 2wt.%), *N* the noble/transition metal (Pd, Pt or Ag), *5M* the transition metal (5wt.% Co or Ag) and *z* the preparation method (WI or SI). The 5Co/Al-SI and 0.5Pd-5Co/Al-SI catalysts used in the present study constitute the second batch of catalysts, which were characterized, evaluated for MOR reaction and compared with the results of the first batch presented in the previous publication, showing great repeatability during the methanol oxidation reaction [39].

4.2. Catalyst Characterization

All catalytic materials were fully characterized regarding their textural and structural properties, via Inductively Coupled Plasma–Atomic Emission Spectroscopy (ICP-AES) in order to measure the metal content (wt.% Co, Ag, Pd and Pt). The surface area, the volume and size of pores of the catalysts were measured in a 300 DV PerkinElmer Optima spectrometer, via N_2 adsorption/desorption experiments (BET method) at −196°C, using an Automatic Volumetric Sorption Analyzer (Nova2200e Quantachrome flow apparatus) . The samples were outgassed overnight at 250°C under vacuum. The X-Ray Diffraction (XRD) diffractograms were accumulated in the range of 10-80° 2θ, with a counting time of 2 sec per step, using a SIEMENS D-500 diffractometer, employing CuKa1 radiation (λ = 0.15405 nm) and operating at 40 kV and 30 mA, in order to determine the structure of the catalysts and the formed metal oxide species (fresh and used catalysts). Scherrer equation (1) was used to calculate the crystallite size of Co_3O_4 phase (D_{XRD}), based on the most intense diffraction peak of Co_3O_4 at 2θ: 35-38°.

 doi:10.20944/preprints202510.1314.v1

$$D_{XRD} = \frac{K\lambda}{\beta \cos\theta} \qquad (1)$$

Where K is Scherrer constant, λ is the wavelength of the X-ray in nm, β is the line broadening and θ is the Bragg angle [52].

Morphological characterization was performed via Scanning Electron Microscope (SEM) imaging, using a JEOL JSM-IT500 microscope. EDS spectra and mapping were obtained using an Oxford Instruments x-Act detector. The samples were embedded in resin, which was grinded and polished, while each resin was gold-plated. The analysis was carried out by applying a voltage of 20 kV.

The reaction mechanism was investigated via temperature-programmed desorption of methanol (TPD-CH_3OH) under 0.1vol.% O_2/He. Initially, the catalysts were saturated with liquid methanol and then the desorption was performed in a fixed bed reactor connected with a mass spectrometer (MS), starting from room temperature (RT) up to 300°C (with a heating rate 10°C/min). The recorded MS signals were: m/z = 31 for CH_3OH, m/z = 45 for DME, m/z = 29 for HCHO and m/z = 44 for CO_2.

Temperature-programmed reduction with H_2 (TPR-H_2) was also used to investigate the reducibility of the catalysts and identity the oxidation states of the metal phases in the fresh and used (after reaction) catalysts. The experiments were performed in the same unit with the desorption studies, while the detailed methodology is described in [39].

4.3. Performance Evaluation

The evaluation of catalysts performance for the methanol oxidation was performed in a bench-scale unit, equipped with a quartz fixed-bed reactor. The reactor was loaded with 0.4 g, using a total gas flow of 600 cm^3/min, corresponding to 40,000 h^{-1} Gas Hour Space Velocity (GHSV). All catalysts were initially screened for methanol oxidation with feed composition: 0.1 vol.% CH_3OH and 0.1 vol.% O_2 balanced with He *(Feed 1)*, in the temperature range: 30-300°C (decreasing temperature mode). The composition of the effluent gases was analyzed using an MKS FT-IR gas analyzer (MG2030, Germany), monitoring continuously CH_3OH and possible reaction products, such as CO_2, H_2O, DME, HCHO, CO, etc. Methanol conversion *(X_{MeOH}, %)* was calculated by the following equation:

$$X_{MeOH} = \frac{[MeOH]_{in} - [MeOH]_{out}}{[MeOH]_{in}} \times 100 \qquad (2)$$

Where $[MeOH]_{in}$ and $[MeOH]_{out}$ are the methanol concentration (ppm) in the inlet and outlet gas streams, respectively.

The optimum catalysts were further evaluated to test their stability in the presence of impurities (CO and/or H_2O) and time-on-stream (TOS). The feed compositions were: 0.1 vol.% CH_3OH- 0.1 vol.% O_2-2 vol.% H_2O *(Feed 2)* and 0.1 vol.% CH_3OH- 0.1 vol.% O_2-2 vol.% H_2O-0.1 vol.% CO *(Feed 3)* balanced with He. The light-off experiments were performed at the same unit and reaction conditions, while the TOS experiments were performed at a constant temperature (T: 230°C) for several hours (TOS: 12h). Water was introduced to the blend of the other gases using a saturation bath at controlled temperature conditions of He flow.

5. Conclusions

The present study moved forward the investigation of Pd-Co/alumina catalysts for the catalytic oxidation of atmospheric pollutants [39], focusing on the methanol oxidation reaction and exploring/improving further the performance and stability of the catalyst. The effect of the noble metal (Pd vs. Pt) and its content (0.5 wt.% vs. 0.1 wt.%) was investigated and the results revealed the superior performance of Pd versus Pt, as even at 0.1 wt.%, Pd had a higher catalytic activity than 0.5wt.% Pt on 5Co/Al-SI catalyst. Different reaction pathways were also followed for each noble metal. The Pd-Co/Al-SI catalyst promoted complete oxidation of methanol to CO_2 and H_2O, while the Pt-Co/Al-SI promoted the partial oxidation to formaldehyde and dehydration to dimethyl ether.

The addition of 2 wt.% Ag on 5Co/Al-SI did not improve its catalyst activity, while the bare 5Ag/Al catalyst showed higher activity than the 5Co/Al catalyst. The synthesis method did not seem

 doi:10.20944/preprints202510.1314.v1

to play a significant role in the case of the Ag-based catalyst, as Ag exhibits mobility during thermal treatments. The incorporation of Pd into the Ag/Al-SI catalyst further increased the oxidation activity of the catalyst, but did not achieve better performance than that of Pd-Co/Al-SI. This is probably related to the interaction and synergistic effect between Pd-metal according to the reduction profiles of the Co-based catalyst, while in the case of Ag-based catalyst palladium seems to enhance the formation of methoxy species, but Ag promote the formation of formaldehyde.

Therefore, the stability of the optimum 0.5Pd-5Co/Al-SI catalyst was finally tested in the presence of CO and/or H_2O. The catalyst performance decreased during light-off experiments, but over time the catalyst activity improved, achieving complete methanol conversion (100%) after 12 h of MOR at T: 230°C. The characterization of the used catalyst revealed that during the stability experiment, in addition to Co_3O_4, the CoO phase was also formed, revealing that the active phase of the catalyst is a mixture of Co_3O_4 and CoO.

Author Contributions: Conceptualization and methodology, E.I. and E.P.; investigation and validation, E.P.; resources A.L.; supervision, E.I. and A.L.; writing—original draft preparation, E.P.; writing—review and editing, E.I. All authors have read and agreed to the published version of the manuscript.

Funding: This research received no external funding.

Data Availability Statement: Data are contained within the article.

Conflicts of Interest: The authors declare no conflicts of interest.

Abbreviations

The following abbreviations are used in this manuscript:

MeOH	Methanol
STP	Standard temperature and pressure
VOCs	Volatile organic compounds
MOR	Methanol oxidation reaction
WI	Wet impregnation
DI	Dry impregnation
SI	Spray impregnation
XRD	X-Ray diffraction
ICP-AES	Inductively coupled plasma–Atomic emission spectroscopy
TPD-CH_3OH	Temperature-programmed desorption of methanol
SEM	Scanning electron microscope
TPR-H_2	Temperature-programmed reduction with H_2
GHSV	Gas hour space velocity
DME	Dimethyl-ether
TOS	Time on stream
JCPDS	Joint Committee on Powder Diffraction Standards
MS	Mass spectrometer
RT	Room temperature

References

1. Ott, J.; Gronemann, V.; Pontzen, F.; Fiedler, E.; Grossmann, G.; Kersebohm, D.B.; Weiss, G.; Witte, C. Methanol, ULLMANN'S encyclopedia of industrial chemistry. Wiley-VCH, 2012. https://doi.org/10.1002/14356007.a16_465.pub3
2. Olah, G.A. Beyond Oil and Gas: The Methanol Economy. *Angew. Chem. Int. Ed.* **2005**, *44*, 2636 –2639. https://doi.org/10.1002/anie.200462121

 doi:10.20944/preprints202510.1314.v1

3. Dalena, F.; Senatore, A.; Basile, M.; Knani, S.; Basile, A.; Iulianelli, A. Advances in Methanol Production and Utilization, with Particular Emphasis toward Hydrogen Generation via Membrane Reactor Technology. *Membranes* **2018**, *8*, 98. https://doi.org/10.3390/membranes8040098
4. Leonzio, G.; Zondervan, E. Carbon Dioxide to Methanol: A Green Alternative to Fueling the Future. *Comp. Methanol Sci.* **2025**, 595-622. https://doi.org/10.1016/B978-0-443-15740-0.00024-0
5. Malik, M.I.; Abatzoglou, N.S.; Achouri, I.E. Methanol to Formaldehyde: An Overview of Surface Studies and Performance of an Iron Molybdate Catalyst. *Catalysts* **2021**, *11*, 893. https://doi.org/10.3390/catal11080893
6. Qian, Q.; Zhang, J.; Cui, M. Synthesis of acetic acid via methanol hydrocarboxylation with CO_2 and H_2. *Nat. Commun.* **2016**, *7*, 11481. https://doi.org/10.1038/ncomms11481
7. Mufarrij, F.; Navarri, P.; Khojasteh, Y. Development and comparative eco-techno-economic analysis of two carbon capture and utilization pathways for polyethylene production. *J. Environ. Chem. Eng.* **2025**, *13(2)*, 115920. https://doi.org/10.1016/j.jece.2025.115920
8. Zadeh, G.R.K.; Panahi, M.; Yasari, E.; Rafiee, A.; Ali Fanaei, M.; Alae, H. Plantwide Simulation and Operation of a Methanol to Propylene (MTP) Process. *J. Taiwan Inst. Chem. Eng.* **2023**, *153*, 105204. https://doi.org/10.1016/j.jtice.2023.105204
9. Bromberg, L.; Cheng, W.K. Methanol as an alternative transportation fuel in the US: Options for sustainable and/or energy-secure transportation, Report, Prepared by the Sloan Automotive Laboratory Massachusetts Institute of Technology Cambridge MA 02139, 2010. https://afdc.energy.gov/files/pdfs/mit_methanol_white_paper.pdf
10. Çelebi, Y.; Aydın, H. An overview on the light alcohol fuels in diesel engines. *Fuel* **2019**, *236*, 890-911. https://doi.org/10.1016/j.fuel.2018.08.138
11. Wang, Y.; Wright, L.A. Comparative Review of Alternative Fuels for the Maritime Sector: Economic, Technology, and Policy Challenges for Clean Energy Implementation. *World* **2021**, *2*, 456–481. https://doi.org/10.3390/world2040029
12. Parris, D.; Spinthiropoulos, K.; Ragazou, K.; Giovou, A.; Tsanaktsidis, C. Methanol, a Plugin Marine Fuel for Green House Gas Reduction—A Review. *Energies* **2024**, *17*, 605. https://doi.org/10.3390/en17030605
13. Giddey, S.; Badwal, S.P.S.; Kulkarni, A.; Munnings, C. Comprehensive review of direct carbon fuel cell technology. *Prog. Energy Combust. Sci.* **2012**, *38(3)*, 360-399. https://doi.org/10.1016/j.pecs.2012.01.003
14. Verhelst, S.; Turner, J.W.G.; Sileghem, L.; Vancoillie, J. Methanol as a fuel for internal combustion engines. *Prog. Energy Combust. Sci.* **2019**, *70*, 43-88. https://doi.org/10.1016/j.pecs.2018.10.001
15. Tian, Z.; Wang, Y.; Zhen, X.; Liu, Z. The effect of methanol production and application in internal combustion engines on emissions in the context of carbon neutrality: A review. *Fuel* **2022**, *320*, 123902. https://doi.org/10.1016/j.fuel.2022.123902
16. Ninomiya, J. S.; Golovoy, A.; Labana, S.S.; Effect of Methanol on Exhaust Composition of a Fuel Containing Toluene, n-Heptane, and Isooctane. *J. Air Pollut. Control Assoc.* **1970**, *20(5)*, 314-317. https://doi.org/10.1080/00022470.1970.10469409
17. Wang, Y.; Jiang, Z.; Wu, Y.; Ai, C.; Dang, F.; Xu, H.; Wan, J.; Guan, W.; Albilali, R.; He, C. Simultaneously Promoted Water Resistance and CO_2 Selectivity in Methanol Oxidation Over Pd/CoOOH: Synergy of Co−OH and the Pd−O_{latt}−Co Interface. *Environ. Sci. Technol.* **2024**, *58*, 18414−18425. https://doi.org/10.1021/acs.est.4c06229
18. Wang, J.; Aguilar-Rios, G.; Wang, R. Inhibition of carbon monoxide on methanol oxidation over g-alumina supported Ag, Pd and Ag–Pd catalysts. *Appl. Surf. Sci.* **1999**, *147*, 44–51. https://doi.org/10.1016/S0169-4332(99)00073-2
19. Yang, Y.; Yu, Y.; Tang, S. Microscopic oxidation reaction mechanism of methanol in H_2O/CO_2 impurities: A ReaxFF molecular dynamics study. *Int. J. Hydrogen Energy.* **2023**, *48(67)*, 26058-26071. https://doi.org/10.1016/j.ijhydene.2023.03.383

 doi:10.20944/preprints202510.1314.v1

20. Fujita, O.; Ito, K.; Catalytic oxidation of unburned methanol with presence of engine exhaust components from a methanol-fueled engine. *Trans. Jpn. Soc. Mech. Eng.* **1988**, *53(495)*, 3454-3458. https://doi.org/10.1299/jsmeb1988.31.2_314
21. Luo, Y.; Xiao, Y.; Cai, G.; Zheng, Y.; Wei, K.; Complete methanol oxidation in carbon monoxide streams over Pd/CeO_2 catalysts: Correlation between activity and properties. *Appl. Catal. B: Environ.* **2013**, *136*, 317-324. https://doi.org/10.1016/j.apcatb.2013.02.020
22. Manzoli, M.; Vindigni, F.; Tabakova, T.; Lamberti, C.; Dimitrov, D.; Ivanov, K.; Agostini, G. Structure-reactivity relationship in Co_3O_4 promoted Au/CeO_2 catalysts for the CH_3OH oxidation reaction revealed by in situ FTIR and operando EXAFS studies. *J. Mater. Chem. A* **2017**, *5*, 2083-2094. http://pubs.rsc.org/en/Content/ArticleLanding/2017/TA/C6TA06442F#!divAbstract
23. Lippits, M.J. Catalytic behavior of Cu, Ag and Au nanoparticles. A comparison, Doctoral Thesis, Universiteit Leiden, The Netherlands, 2010. https://hdl.handle.net/1887/16220
24. Zafeiratos, S.; Dintzer, T.; Teschner, D.; Blume, R.; Hävecker, M.; Knop-Gericke, A.; Schlögl, R. Methanol oxidation over model cobalt catalysts: Influence of the cobalt oxidation state on the reactivity. *J. Catal.* **2010**, *269*, 309-317. https://doi.org/10.1016/j.jcat.2009.11.013
25. Zhang, X.; Chen, X.; Liu, Y.; Guo, M. Effects of Support on Performance of Methanol Oxidation over Palladium-Only Catalysts. *Water Air Soil. Pollut.* **2020**, *231*, 277. https://doi.org/10.1007/s11270-020-04656-1
26. Santoveña-Uribe, A.; Ledesma-Durán, A.; Torres-Enriquez, J.; Santamaría-Holek, I. Theoretical Insights into Methanol Electro-Oxidation on NiPd Nanoelectrocatalysts: Investigating the Carbonate–Palladium Oxide Pathway and the Role of Water and OH Adsorption. *Catalysts* **2025**, *15*, 101. https://doi.org/10.3390/catal15020101
27. Gupta, S.; Fernandes, R.; Patel, R.; Spreitzer, M.; Patel, N.H. A review of cobalt-based catalysts for sustainable energy and environmental applications. *Appl. Catal. A: Gen.* **2023**, *661*, 119254. https://doi.org/10.1016/j.apcata.2023.119254
28. Karatok, M.; Sensoy, M.G.; Vovk, E.I.; Ustunel, H.; Toffoli, D.; Ozensoy, E. Formaldehyde Selectivity in Methanol Partial Oxidation on Silver: Effect of Reactive Oxygen Species, Surface Reconstruction, and Stability of Intermediates. *ACS Catal.* **2021**, *11*, 6200−6209. https://doi.org/10.1021/acscatal.1c00344
29. Quaglio, M.; Bezzo, F.; Gavriilidis, A.; Cao, E.; Al-Rifai, N.; Galvanin, F. Identification of kinetic models of methanol oxidation on silver in the presence of uncertain catalyst behavior, *AIChE J.* **2019**, *65*, 16707. https://doi.org/10.1002/aic.16707
30. Jabłonska, M.; Nocun, M.; Bidzinska, E. Silver–Alumina Catalysts for Low-Temperature Methanol Incineration. *Catal. Lett.* **2016**, *146*, 937–944. https://doi.org/10.1007/s10562-016-1713-x
31. Lykaki, M.; Pachatouridou, E.; Iliopoulou, E.; Carabineiro, S.A.C.; Konsolakis, M. Impact of the synthesis parameters on the solid-state properties and the CO oxidation performance of ceria nanoparticles. *RSC Adv.* **2017**, *7*, 6160. https://doi.org/10.1039/C6RA26712B
32. Darda, S.; Pachatouridou, E.; Lappas, A.; Iliopoulou, E. Effect of Preparation Method of Co-Ce Catalysts on CH_4 Combustion. *Catalysts* **2019**, *9*, 219. https://doi.org/10.3390/catal9030219
33. Akarmazya, S.S.; Panagiotopoulou, P.; Kambolis, A.; Papadopoulou, C.; Kondarides, D.I. Methanol dehydration to dimethylether over Al_2O_3 catalysts, *Appl. Catal. B: Environ.* **2014**, *145*, 136–148. http://dx.doi.org/10.1016/j.apcatb.2012.11.043
34. Luo, Y.; Qian, Q.; Chen, Q. On the promoting effect of the addition of $Ce_xZr_{1-x}O_2$ to palladium based alumina catalysts for methanol deep oxidation. *Mater. Res. Bull.* **2015**, *62*, 65–70. http://dx.doi.org/10.1016/j.materresbull.2014.11.025
35. Guo, Y.; Zhang, S.; Mu, W.; Li, X.; Li, Z. Methanol total oxidation as model reaction for the effects of different Pd content on Pd-Pt/CeO_2-Al_2O_3-TiO_2 catalysts. *J. Mol. Catal. A Chem.* **2017**, *429*, 18–26. http://dx.doi.org/10.1016/j.molcata.2016.11.041
36. Cordi, E.M.; Falconer, J.L. Oxidation of Volatile Organic Compounds on Al_2O_3, Pd/Al_2O_3, and PdO/Al_2O_3 Catalysts. *J. Catal.* **1996**, *162*, 104-117. https://doi.org/10.1006/jcat.1996.0264

 doi:10.20944/preprints202510.1314.v1

37. Jabłońska, M.; Król, A.; Kukulska-Zając, E.; Tarach, Girman, V.; Chmielarz, L.; K.; Góra-Marek, K. Zeolites Y modified with palladium as effective catalysts for low-temperature methanol incineration. *Appl. Catal. B: Environ.* **2015**, *166–167*, 353–365. , http://dx.doi.org/10.1016/j.apcatb.2014.11.047
38. Brewer, T.F.; Abraham, M.A.; Silver, R.G. Mixture Effects and Methanol Oxidation Kinetics over a Palladium Monolith Catalyst. *Ind. Eng. Chem. Res.* **1994**, *33*, 526-533. https://pubs.acs.org/doi/10.1021/ie00027a009
39. Iliopoulou, E.F.; Pachatouridou, E.; Lappas, A.A. Novel Nanostructured Pd/Co-Alumina Materials for the Catalytic Oxidation of Atmospheric Pollutants. *Nanomaterials* **2024**, *14*, 124. https://doi.org/10.3390/nano14010124
40. Sun, J.; Wang, H.; Zhao, M. Porous Co_3O_4 column as a high-performance Lithium anode material. *Journal of Porous Materials* **2021**, *28*, 889–894. https://doi.org/10.1007/s10934-021-01041-z
41. Baylet, A.; Marecot, P.; Duprez, D.; Castellazzi, P.; Groppi, G.; Forzatti, P. In situ Raman and in situ XRD analysis of PdO reduction and Pd^0 oxidation supported on γ-Al_2O_3 catalyst under different atmospheres. *Phys. Chem. Chem. Phys.* **2011**, *13*, 4607–4613. https://doi.org/10.1039/C0CP01331E
42. Keijzer, P.H.; E. van den Reijen, J.; Keijzer, C.; P. de JONG, K.; E. de Jongh, P. Influence of atmosphere, interparticle distance and support on the stability of silver on a-alumina for ethylene epoxidation. *J. Catal.* **2022**, *405*, 534–544. https://doi.org/10.1016/j.jcat.2021.11.016
43. Das, S.; Kahnt, M.; van Valen, Y.; Bergh, T.; Blomberg, S.; Lyubomirskiy, M.; Schroer, C.G.; Venvik, H.J.; Sheppard, T.L. Restructuring of Ag catalysts for methanol to formaldehyde conversion studied using in situ X-ray ptychography and electron microscopy. *Catal. Sci. Technol.* **2024,** *14*, 5885. https://doi.org/10.1039/D4CY00770K
44. Chanerika, R.; Shozi, M.L.; Friedrich, H.B. Synthesis and Characterization of Ag/Al_2O_3 Catalysts for the Hydrogenation of 1-Octyne and the Preferential Hydrogenation of 1-Octyne vs 1-Octene. *ACS Omega* **2022**, *7*, 4026−4040. https://doi.org/10.1021/acsomega.1c05231
45. Ousji, R.; Ksibi, Z.; Ghorbel, A.; Fontaine, C. Ag-Based Catalysts in Different Supports: Activity for Formaldehyde Oxidation, *Adv. Mater. Phys. Chem.* **2022**, *12*, 163-176. https://www.scirp.org/journal/ampc
46. Guldur, C.; Balikci, F. Catalytic oxidation of CO over Ag-Co/alumina catalysts. *Chem. Eng. Comm.* **2003,** *190*, 986998. https://doi.org/10.1080/00986440390207567
47. Cordi, E.M.; Falconer, J.L. Oxidation of volatile organic compounds on a $Ag/A1_2O_3$ catalyst. *Appl. Catal. A: Gen.* **1997,** *151*, 179-191. https://doi.org/10.1016/S0926-860X(96)00264-5
48. James, O.O.; Maity, S. Temperature programme reduction (TPR) studies of cobalt phases in γ-alumina supported cobalt catalysts. *J. Pet. Technol. Altern. Fuels* **2016**, *7*, 1-12. https://doi.org/10.5897/JPTAF2015.0122
49. Deori, K.; Deka, S. Morphology oriented surfactant dependent CoO and reaction time dependent Co_3O_4 nanocrystals from single synthesis method and their optical and magnetic properties. *Cryst. Eng. Comm.* **2013,** *15*, 8465. https://doi.org/10.1039/C3CE41502C
50. Natile, M.M.; Glisenti, A. Study of Surface Reactivity of Cobalt Oxides: Interaction with Methanol. *Chem. Mater.* **2002**, *14*, 3090-3099. https://doi.org/10.1021/cm0211150
51. Wang, W.; Seiler, M.; Hunger, M. Role of Surface Methoxy Species in the Conversion of Methanol to Dimethyl Ether on Acidic Zeolites Investigated by in Situ Stopped-Flow MAS NMR Spectroscopy. *J. Phys. Chem. B* **2001**, *105*, 12553-12558. https://doi.org/10.1021/jp0129784
52. Patterson, A.L. The Scherrer Formula for I-Ray Particle Size Determination. *Phys. Rev.* **1939**, *56*, 978-982. https://journals.aps.org/pr/pdf/10.1103/PhysRev.56.978